UNIVERSITY OF HELSINKI

https://helda.helsinki.fi

Helda

Using the site-knockout strategy to understand the low activity of the nitrate electro-reduction reaction on Pt(111)

da Silva, Kaline Nascimento

Royal Society of Chemistry
2022-06-27

da Silva, K N, Soffiati, G, da Silva, E Z, San-Miguel, M A & Sitta, E 2022, 'Using the site-knockout strategy to understand the low activity of the nitrate electro-reduction reaction on Pt(111)', New Journal of Chemistry, vol. 46, no. 25, pp. 12132-12138. https://doi.org/10.1039/d2nj01773c

http://hdl.handle.net/10138/358016
10.1039/d2nj01773c

acceptedVersion

Downloaded from Helda, University of Helsinki institutional repository.

This is an electronic reprint of the original article.

This reprint may differ from the original in pagination and typographic detail.

Please cite the original version.

Using the site-knockout strategy to understand the low activity of nitrate electro-reduction reaction on Pt(111)

Kaline Nascimento da Silva[a,b], Gabriela Volpini Soffiati[c], Edison Z. da Silva[d], Miguel Angel San-Miguel[c] and Elton Sitta[a,]*

a Chemistry Department, Federal University of Sao Carlos, Rod. Washington Luis, km 235, Sao Carlos, Brazil. ZIP code 13565-905

b Department of Chemistry, University of Helsinki, A.I. Virtasen aukio 1, 00560, Finland (present address)

c Institute of Chemistry, State University of Campinas, ZIP code 13083-970, Campinas, SP, Brazil

d Institute of Physics "Gleb Wataghin", State University of Campinas, 13083-859, Campinas - SP, Brazil

**e-mail: esitta@ufscar.br*

Graphical Abstract

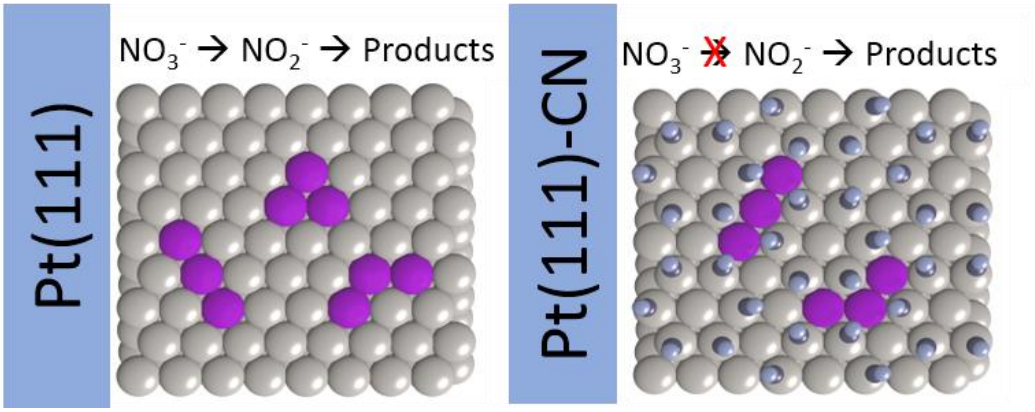

Abstract

Nitrate and nitrite reduction reactions (NO_3RR and NO_2RR, respectively) are important processes in water treatment as well as model processes in surface science. The sluggish kinetics observed for NO_3RR on Pt electrodes is usually explained by the difficulty in removing NO_{ad}. However, NO_2RR shares this same intermediate and depicts higher activity in the same experimental conditions. Herein, we employed the site block strategy to show that nitrate demands contiguous Pt sites to be converted into nitrite and then to NO_{ad}. Both NO_3RR and NO_2RR were studied at Pt(111) and Pt(111) modified with cyanide ions (Pt(111)-CN). While NO_2RR depicted lower activity in Pt(111)-CN than in Pt(111), NO_3RR is completely inhibited. Regardless of the presence of cyanide, DFT-based analysis revealed that both NO_3 and NO_2 adsorption could occur on the bidentate form. Still, after this step, extra contiguous sites should be provided to NO_{3ad} proceeds with the reduction reaction, which is not available on Pt(111)-CN. These results bring experimental evidence that the nitrate to nitrite conversion is an important bottleneck on NO_3RR, and the presence of NO_{ad} (produced as intermediate during NO_3RR) unfavored this step by geometric factors.

Keywords: nitrate reduction; nitrite reduction; Pt(111); DFT calculations; atomic ensemble effect.

Introduction

The industrial production of nitrogen fertilizers has been causing an increase of soluble nitrogen-containing species above the rate of microbiological denitrification capacity.[1,2] Part of this imbalance of nitrogen cycle results in nitrate accumulation in sewers and industrial wastewater, leading to groundwater contamination.[3,4] Moreover, the excess of nitrate consumption by humans can cause some severe diseases, becoming important the development of methods to reduce the nitrate levels in the environment, especially from aqueous solutions.[5]

Reactions involving nitrogenous compounds show high complexity due to a large number of stable species with nitrogen atoms adopting oxidation numbers from -3 to +5.[6] These species can react between them, resulting in a complex mechanism with several chemical and electrochemical steps and different pathways. Therefore, electrochemistry plays a central role in designing catalysts with high selectivity for desired products, with low toxicity (like N_2) or contributing to industrial processes, such as hydroxylamine, nitric oxide, or ammonia, providing an alternative route to the Haber-Bosch method.[3]

The nitrate reduction reaction (NO_3RR) mechanism on Pt has been extensively studied in recent decades.[7–15] The main reaction steps for low nitrate concentration are summarized in Figure 1. After the nitrate ($NO_{3(ad)}$) adsorption, nitrite ($NO_{2(ad)}$) and $NO_{(ad)}$ are the first and second reduction products on Pt(111) at $E < 0.25$ V and $E < 0.60$ V, respectively. $NO_{(ad)}$ is a stable species on Pt, competing with both Pt-H and Pt-OH formations and maintaining the catalyst surface partially poisoned in the potential window from hydrogen to oxygen evolution reactions. $NO_{(ad)}$ reduction occurs below 0.40 V[16] via a Langmuir-Hinshelwood mechanism with the hydrogen presence on the surface (Pt-H) or via an Eley-Rideal mechanism with direct proton transfer from the solution depending on hydrogen

availability at the electrode surface. There is no consensus about the first NO reduction intermediate because NOH and NHO have almost the same adsorption energy,[17] whereas the further steps of NO reduction will culminate on the ammonium or hydroxylamine formation[18] as the main NO_3RR products on Pt and acidic electrolytes as observed by FTIR[19–21] and DEMS.[22]

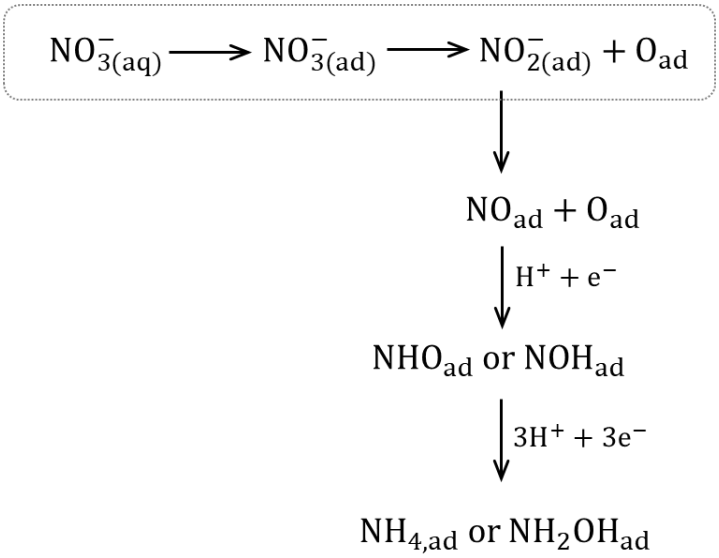

Figure 1 – Main steps during the nitrate reduction reaction.

The Nitrite Reduction Reaction (NO_2RR) can be studied from NO_2^- dissolution directly into the supporting electrolyte. On Pt(111), NO_2RR displays a higher current than NO_3RR, concluding that the nitrate conversion to nitrite steps (as highlighted in Figure 1) is the reaction rate-determining step (RDS) under acidic conditions.[21] To gain insights into the mechanism's complexity and aid in investigating the electrochemical steps and the different reaction pathways, density functional theory (DFT) calculations appear as an essential tool to reveal critical information at the atomic level.[15,23–26]

In the present work, we studied the effect of available continuous sites on the first NO_3RR steps. Therefore, we modified Pt(111) with cyanide ions (Pt(111)-CN), forming hexagonal patterns,[27,28] where the CN groups are adsorbed on top of platinum atoms through the carbon atom.[29,30] As a result of this modification, all three contiguous Pt

atoms vanish from the Pt(111) surface, but the electronic properties of the Pt atoms that remain free are kept unchanged.[31] Thus, this modification is doubtless a tool for mechanism understanding. The nitrate and nitrite adsorption were also simulated employing density functional theory (DFT) calculations on both Pt(111) and Pt(111)-CN surfaces.

Experimental

The single-crystal surface preparation method was previously described in ref.[32], and the surface activation procedure in ref.[33] The working electrode area was estimated as 0.0450 cm^2. 0.1 M of $HClO_4$ solution was prepared diluting ultrapure $HClO_4$ (ACS reagent – 70 % Sigma-Aldrich) in 18.2 MΩ cm water (Milli-Q system) and served as supporting electrolyte. Sodium nitrate (Sigma-Aldrich, 99,995%) or sodium nitrite (ACS reagent, Ph. Eur., 99%) were added into the electrolyte from 1 M stock solution yielding the desired concentrations. An Autolab PGSTAT 128 N equipped with Scan 250 modulus was used as a potentiostat. Before the experiments, the solution was purged with Argon 5.0 N, and during the data collection, this gas was kept in the cell headspace. The surface quality was checked by a 0.05 V s^{-1} cyclic voltammetry from 0.05 to 0.9 V.

Cyanide-modified Pt(111) electrode (Pt(111)-CN) was prepared by immersion of a clean and well-ordered Pt(111) surface in a 0.1 M KCN (ACS reagent, Ph. Eur., 97%) solution for approximately 3 min, rinsed with ultrapure water and transferred to the electrochemical cell containing cyanide-free 0.1 M $HClO_4$, as described in [34].

NO-saturated adlayers were *ex-situ* prepared by immersion of the clean and well-ordered Pt(111) electrode in a 0.1 M $HClO_4$ solution containing 0.01 M $NaNO_2$ for 3 min.[17] Applying the same procedure to a cyanide-modified Pt(111) electrode yielded mixed CN–

NO adlayers. After the NO adlayer formation, the electrode was rinsed with ultrapure water and transferred to the electrochemical cell containing 0.1 M $HClO_4$ and polarized at 0.85 V. The NO stripping was made with a scan rate of 2 mV s^{-1}.

Computational simulations

DFT simulations were performed using the Vienna Ab initio Simulation Package (VASP).[35–38] The Perdew–Burke–Ernzerhof (PBE)[39,40] functional within the generalized gradient approximation (GGA) was used to treat the exchange-correlation effects and the interactions between the nuclei and the core electrons were considered with the projector augmented wave (PAW) method.[41] An energy cut-off of 450 eV for the plane-wave basis was used in all systems.

A bulk lattice parameter of 3.967 Å (1.2 % different from the literature value[42]) was found for Pt fcc cell. Both Pt(111) and Pt(111)-CN surfaces were modeled as a $(2\sqrt{3}x2\sqrt{3})R30^{o}$ slab with five platinum layers and 20 Å of vacuum to avoid interactions between adjacent slabs along the surface normal. Pt(111)-CN was constructed by placing six CN groups forming a hexagonal configuration on the clean Pt(111) surface, a model based on both experimental[27,28] and theoretical[43] studies. NO_x molecules were approximated to both surfaces to calculate the adsorption energies. The free molecules were optimized in an asymmetric box of 11x9x12 $Å^3$.

During the optimization process, the two bottom Pt layers were fixed to reproduce the bulk behavior. Convergence criteria of 10^{-8} eV for the energy and 0.01 eV/Å for the forces were used. The Brillouin zone was sampled using the Monkshorst-Pack method with a 4x4x1 k-points mesh, during relaxations, for both surfaces and adsorption systems, and only the gamma point was used for the free NO_X molecules. Dipole corrections along the

z-axis were applied since the presence of the adsorbates creates asymmetry in the terminations of the slab. Atomic charges were computed using the Bader charge density analysis as implemented by Henkelman and co-workers.[44] The charge density differences, $\Delta\rho_{ads}$, were calculated as Equation 1

$$\Delta\rho_{ads} = \rho_{tot} - \rho_{surf} - \rho_{mol} \quad \text{Equation 1}$$

where ρ_{tot}, ρ_{surf}, ρ_{mol} are the charge densities of the whole adsorption system, the surface, and the adsorbed molecule at the same geometries as the whole system, respectively.

The calculations included NO_2 and NO_3 molecules (NO_x) bonded to Pt atoms on Pt(111) and Pt(111)-CN surfaces (NO_x*), as represented by the Reaction 1 with * denoting a surface adsorption site. The adsorption energies were obtained, as Equation 2, following the generalized chemical reaction also presented below. $U_{NOx\text{-}Pt}$ is the energy for the adsorption systems containing surface and molecule, U_{NOx} is the free nitrogen oxide energy, and U_{Pt} is the clean surface energy. Since all computed and referenced adsorption energies in this work are negative (favorable), they will be reported as positive values to clarify the discussions.

$$NO_X + * \rightarrow NO_X^* \quad \text{Reaction 1}$$

$$U_{ads} = U_{NOx-Pt} - U_{Pt} - U_{NOx} \quad \text{Equation 2}$$

Results

Nitrate and Nitrite electrochemical reduction on Pt(111)

Figure 2(A) compares the NO_3^- and NO_2^- (both at 10 mM) interactions with Pt(111). The cyclic voltammograms (CV) in absence of these species (blank curves) are also shown in

dotted black lines. In the absence of NO_3^-/NO_2^- it is possible to recognize the well-defined processes on Pt(111)|H_2O interfaces namely: a broad-flat region between 0.050 and 0.375 V due to Pt-H adsorption/desorption on {111} domains covering up to 66% of the surface[45] and the so-called butterfly region from 0.60 to 0.90 V consisting of Pt-OH formation/stripping from water discharge with a characteristic couple of peaks at 0.80 V.[32] The Pt-H and Pt-OH regions are split by a small-current region of water-surface interactions. The current density values, as well as the absence of peak on Pt-H region, fully agree with the literature[32] and it attests both good surface orientation and solution cleanness.

The presence of nitrate (10 mM) in the electrolyte causes competition with both Pt-H and Pt-OH formation, and the overall current becomes lower than those observed on the blank curve on the Pt-OH region due to the presence of strongly adsorbed nitrate intermediates. Moreover, two reduction processes (a peak at 0.35 and a wave at E < 0.20 V) can be observed during negative-going scan on Pt(111) (see SI files for better visualization), and they are usually explained by the NO_{ad} reduction at on-top and three-fold hollow sites, respectively[46] (see the discussion below). The NO_{ad} is stable and requires high overpotentials for its reduction.[16] Close to zero reaction order (*n*), estimated by the current-dependence with nitrate concentration (shown in SI files), confirms that the overall process is controlled by the reduction of NO_3^- intermediates adsorbed on the surface instead of direct nitrate reduction, in agreement with the literature.[47]

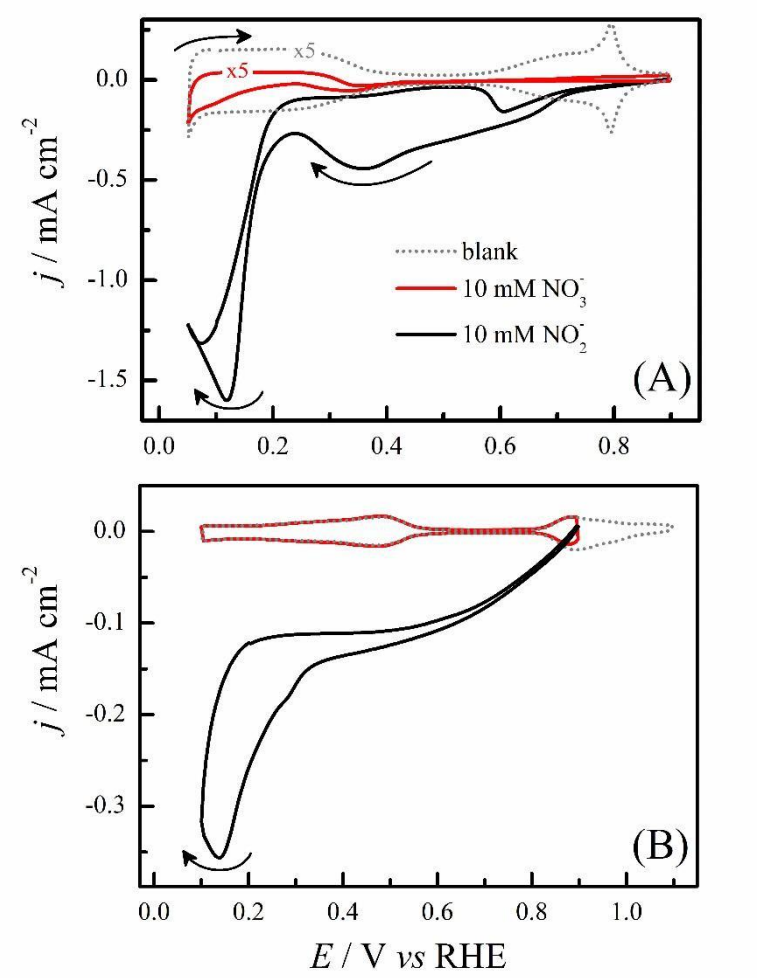

Figure 2 (A) Pt(111) cyclic voltammograms at 0.01 V s^{-1} in 0.1 M $HClO_4$ + 10 mM $NaNO_3$ (red) or 10 mM $NaNO_2$ (black). Dotted lines represent the Pt(111) blank cyclic voltammograms at 0.05 V s^{-1} i.e. in absence of both $NaNO_3$ and $NaNO_2$. (B) Pt(111)-CN cyclic voltammograms in the same solution conditions of (A). The arrows indicate the sweep direction.

When nitrate is replaced by nitrite ions, the currents become one order higher. During the negative-going scan, two main processes can be observed; namely, a broad region that starts at 0.60 V with maximum current density value (j_{max}) around 0.40 V and a sharp peak in the Pt-H region with j_{max} at 0.10 V. In Pt(*poly*), the broad region and sharp peak are related to the N_2O and hydroxylamine production, respectively[48]. In contrast to NO_3RR, the CV currents for NO_2RR depend on the nitrite concentration yielding an n = 0.60 at 0.15 V (shown on SI files).

The cyanide presence on Pt(111) surface (Figure 2(B)) still allows the Pt-H and Pt-OH adsorption, however, they happen in a wide potential window and the Pt-OH region loses the pair of peaks at 0.8 V, in accordance with results previously reported in ref.[49]. While the nitrate is able to interact with Pt(111) surfaces, its reduction is strongly inhibited in Pt(111)-CN as observed in Figure 2(B), in which the current profile for Pt(111)-CN|H_2O system (dotted line) is the same for Pt(111)-CN|H_2O,NO_3^-. On the other hand, when compared to Pt(111), the NO_2RR on Pt(111)-CN has a lower activity in the overall potential window; however, it is still possible to recognize the broad process at the high potential that is replaced by a peak with the increase of H_{ad} coverage. The maximum potential was set at 0.9 V in the presence of nitrate and nitrite to avoid the nitrite oxidation or the oxidation of adsorbed species.

While the CN adsorption onto Pt(111) decreases the number of exposed Pt atoms by 50%,[49] the current inhibition during NO_2RR is 80% at 0.15 V peak, highlighting the site blockage effect is able to inhibit some reaction pathways. For the sake of comparison, Figure 3 brings NO_2RR and reductive NO_{ad} stripping [46] on both Pt(111) and Pt(111)-CN. On Pt(111), the NO saturation coverage is ca. 0.4-0.5 ML[46,50], and the NO_{ad} reduction reaction (NORR) occurs via the well-defined four processes: a peak about 0.28 V and a shoulder at 0.34 V, which refers to the reduction of NO adsorbed in on-top sites;[46] a peak at ca 0.15 V that corresponds to the reduction of NO adsorbed on three-fold hollow sites,[51,52] and finally, a peak in 0.77 V that is not well-described in the literature. These first three processes correspond to the peaks observed during NO_2RR on Pt(111), and possibly the above-cited processes contribute enormously to NO_2RR. On Pt(111)-CN, only the processes at 0.77 and 0.21 V are observed during NORR, i.e., only the NO reduction on on-top sites is maintained[46]. Furthermore, the comparison between NORR

and NO_2RR on Pt(111)-CN shows that the NO_2RR activity from 0.80 to 0.40 V seems to happen not only via the NO pathway but through other N_xO_y species.

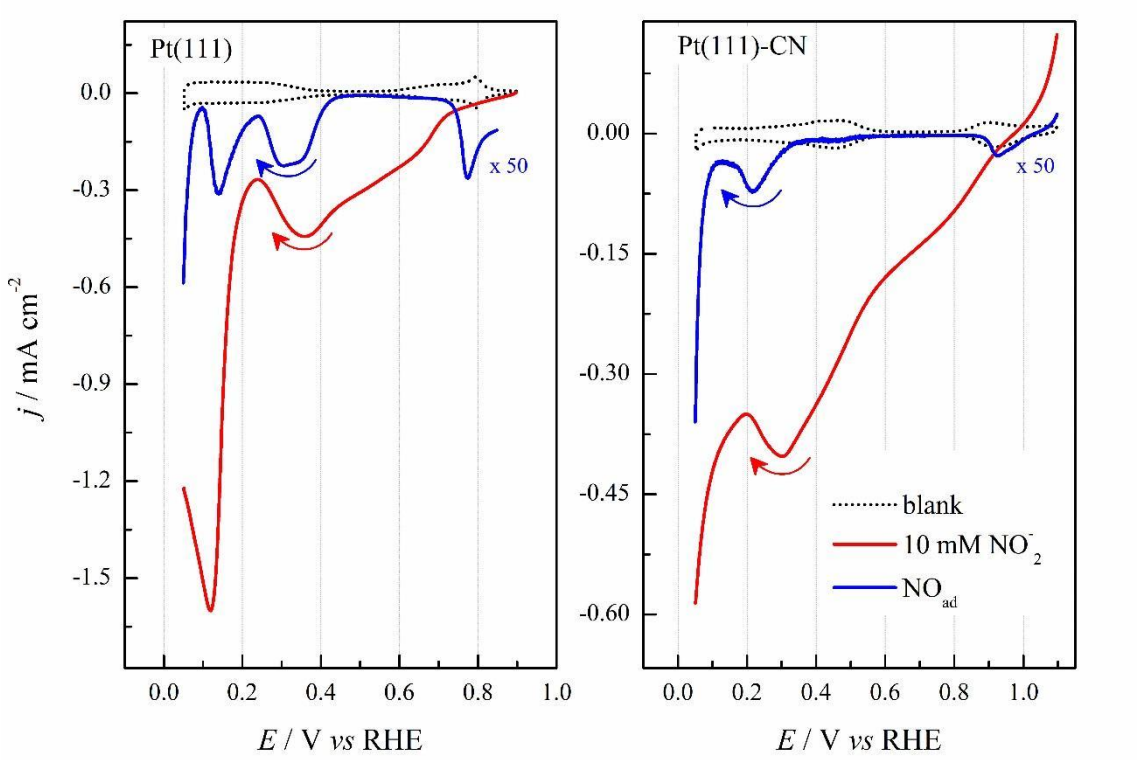

Figure 3 Cyclic voltammogram in 0.1 M $HClO_4$ (black) with addition 10 mM $NaNO_2$ (red) at 10 mV s^{-1} and NO stripping (blue) at 2 mV s^{-1} on Pt(111) and Pt(111)-CN, respectively.

Density functional theory for nitrate and nitrite adsorption

Nitrate can be adsorbed on the surface in a monodentate, bidentate, or tridentate way, i.e., binding through one, two, or three oxygen atoms. The literature shows that the bidentate configuration is the most stable one when Au, Ag, and Pt are used,[25,53] and it can be observed with spectroscopic experiments in Pt(*poly*) surface.[52] With the bidentate nitrate configuration, DFT calculations[15] using stepped {211} surfaces showed that the adsorption energy for nitrate on a {111} terrace is 2.23 eV while the nitrite adsorption

energy is 1.93 eV, which is a piece of evidence about the difference in adsorption strength between both species.

The bidentate adsorption of NO_2 and NO_3 species on the Pt(111) surface was simulated using DFT calculations, as can be seen in Figure 4, where nitrite has adsorption energy of 1.38 eV, while nitrate shows 1.70 eV, and these results are consistent with reported values in the literature.[25] However, when the nitrogen oxide molecules were placed in the middle sites of Pt(111)-CN, the adsorption energies decreased, following the same trend in which the NO_3 adsorption is still more favorable ca. 0.3 eV than the NO_2, with adsorption energies of 1.22 eV and 0.95 eV, respectively. This change in adsorption energies is expected and could cause a decrease in the activity of NO_2RR and NO_3RR on Pt(111)-CN, once the adsorption process of the active species is less favorable when the surface is partially covered with cyanide, but it does not explain why the nitrate reduction is completely inhibited.

Thus, we carry out simulations with the NO_3 adsorption in tridentate mode, which is favorable on Pt(111), with adsorption energy ca. 1.16 eV, but it is impeded in Pt(111)-CN because of the lack of available Pt sites.

The net electron transfer from the surface to the adsorbed molecules was calculated from the Bader charges for every system. As can be seen in Figure 4, the decrease in adsorption energy when the CN- groups are present on the surface, can be explained by the reduction in the electron transfer, which also can be visualized in the electron density difference plots reported.

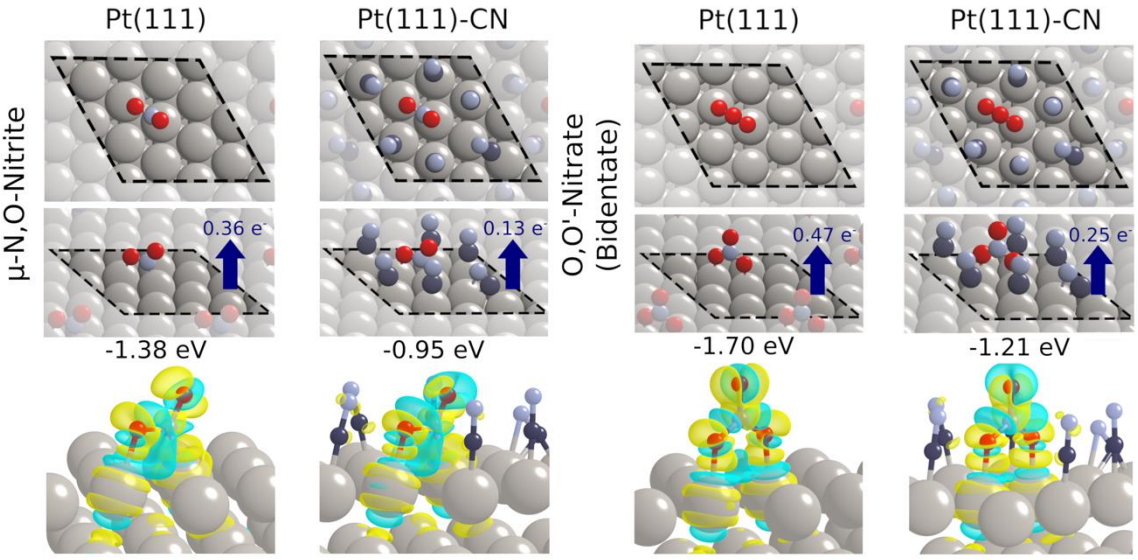

Figure 4 - NO_x adsorption configurations on Pt(111) and Pt(111)-CN surfaces. The left panel corresponds to μ-N,O-Nitrite configuration where NO_2 bonds to two superficial Pt atoms through N and O atoms. The right panel refers to the bidentate adsorption mode (O,O`-Nitrate) in which the NO_3 molecule bonds to two Pt atoms through two oxygen atoms. For each system, top and side views are represented and the adsorption energies and the charge transfer flux are also reported. Bottom panels show the electron charge density differences, where yellow and blue regions correspond to accumulation and depletion of charge, respectively.

Discussion

The higher currents observed during NO_2RR when compared to NO_3RR could be explained by the fast conversion of NO_2^- into NO_{ad}. Additionally, in acidic media, NO_2^- is involved in several chemical equilibriums[17] yielding HNO_2, NO, N_2O, NO_2, N_2O_4, NO_3^- and NO^+, which could provide other active species to be electrochemically reduced. Specifically, it is expected that the electroreduction reactions of neutral molecules that weakly interact with the surface,[54] for example N_2O, will have their maximum activity near the potential of zero charge on Pt surfaces,[55,56] i.e., around 0.30 V for Pt(111) in the experimental conditions employed in this work.[32] Unfortunately, this potential region also corresponds to the $NO_{(ad)}$ reduction becoming difficult to infer about the active species in

solution. The same discussion could be drawn to NO_3RR, considering the NO_3^-/HNO_3 equilibrium.[57] Regardless of the active species in solution (NO_3^-/HNO_3 or $NO_2^-/HNO_2/NO_2/N_2O_4$), after the adsorption, in NO_3RR, the species containing three oxygens should be converted into species with two oxygens and then into $NO_{(ad)}$. After this point, NO_3RR and NO_2RR share common intermediates.

Using the site-knockout strategy employing cyanide adsorption, while NO_2RR is partially inhibited, we observe the complete extinguishment of NO_3RR on Pt(111)-CN. The well-known cyanide adsorption on Pt(111) modifies the sizes of the adsorbing sites at molecular level as shown in Figure 5 in which it is possible to highlight three types of sites containing three Pt atoms: linear sites (a), angular sites (b) and contiguous sites (c). While in the presence of CN_{ad}, the sites (a) and (b) are maintained, the sites (c) vanish from the surface.

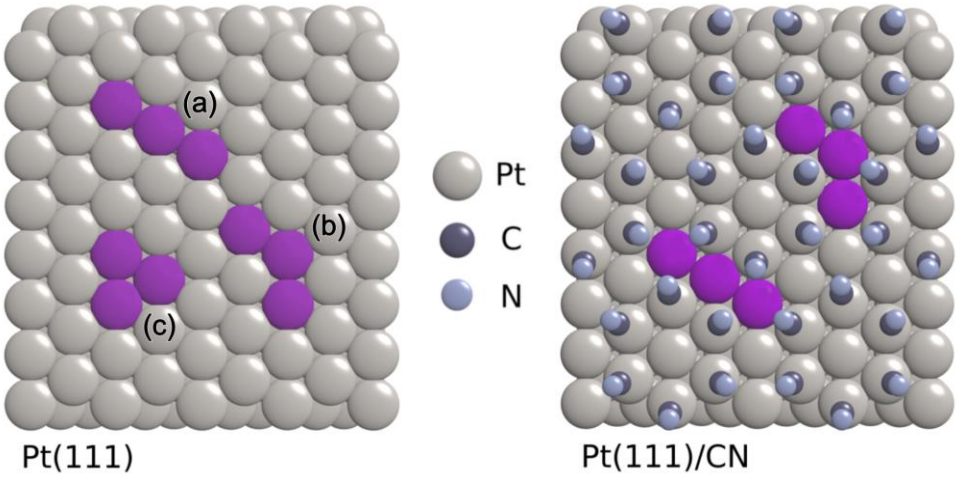

Figure 5 - Hard sphere model of a clean Pt(111) surface (left) and modified with cyanide (right), indicating the possible arrangement of three connected Pt atoms. Adapted from [58]

These results suggest that the nitrite or other active species present in the solutions demand only two contiguous surface sites or type-(a) or (b) sites with three Pt atoms to react, providing the currents observed during NO_2RR. On the other hand, type-(c) sites

are essential to nitrate reduction. DFT studies revealed that nitrate and nitrite adsorption occur by the two oxygen atoms in both Pt(111) and Pt(111)-CN; however, the nitrate adsorption by the three oxygen atoms is only possible in Pt(111). Thus, we can conclude that after the initial adsorption in bidentate, according to the spectroscopy evidence,[52] NO_{3ad} demands an extra contiguous site to be converted into nitrite. This extra site can be used to the adsorption of the third-oxygen of the nitrate ion as suggested previously by Goldsmith and co-workers[15] for nitrate dissociation on Pt(211), or the hydrogen adsorption that will react with the oxygen of the adsorbed nitrate during the nitrate to nitrite conversion step. It is important to point out that according to DFT studies in ref. [25], the free NO_3 shows three 1.252 Å equivalent bonds, while in O,O-nitrate adsorption mode there is a lenght-bond change due to the interaction with {111} surface, a 1.222 Å and two 1.306 Å bonds. However, after the adsorption in tridentate mode, all three bonds show 1.291 Å, considering that the NO_3 is parallel to the surface, this adsorption mode is not active in infrared experiments, which represents an experimental limitation to confirm that nitrate should be adsorbed on surface by the three oxygen atoms to be converted to nitrite.

During both NO_3RR and NO_2RR, NO_{ad} is an intermediate undoubtedly present on the surface[22]; however, more than an intermediate that demands a high overpotential to be reduced, randomized NO_{ad} molecules on surface block sites in different ways, including the extinguishment of type-(c) sites. In the case of NO_2RR, even at high NO_{ad} coverages, the reaction can occur in small size sites, as observed in Pt(111)-CN. On the other hand, when a clean Pt(111) surface is in contact with the electrolyte in the presence of nitrate, NO_{ad} is produced, which decreases the sites size to further nitrate adsorption. Thus, the nitrate to nitrite conversion becomes unviable. This self-surface poisoning caused by NO_3^- could explain the low activity for NO_3RR on Pt. The literature reports examples of

reactions where intermediates act as surface poisons to reactant adsorption, such as the NO_{ad} during the ammonia oxidation reaction, that probably causes the inhibition of the N-N coupling reaction[59] and the CO_{ad} during the oxidation of small organic molecules.[60]

Conclusions

The nitrate (NO_3RR) and nitrite (NO_2RR) reduction reactions were studied in both well-oriented Pt(111) and cyanide modified Pt(111) surfaces in non-adsorbing anion electrolyte. While NO_2RR provides the highest reduction current and activity on Pt(111), NO_3RR displays a sluggish kinetic on Pt(111) and is completely inhibited on Pt(111)-CN. DFT results indicate that both nitrite and nitrate adsorption can occur on clean Pt(111) and Pt(111)-CN in the bidentate form, which let us conclude that the nitrate to nitrite conversion demands at least three contiguous sites. Similarly, the effect caused by CN_{ad}, the NO_{ad} produced as intermediate during NO_3RR, could be acting as a surface site blocker, decreasing the number of three contiguous Pt sites on the surface and explaining the poor NO_3RR activity when compared with NO_2RR. This work brings an important geometric factor at the molecular level during NO_3RR, which can provide insights for the design of new catalysts.

Acknowledgments

The authors thank The São Paulo Research Foundation (FAPESP) for financial support (#2013/07296-2, #2017/11986-5, #2016/23891-6, #2017/26105-4) and Shell and the strategic importance of the support given by ANP (Brazilian National Oil, Natural Gas and Biofuels Agency) through the R&D levy regulation. KNS and GVS thank Brazilian Council for Scientific and Technological Development (CNPq) for the scholarship (#141097/2018-3 and #142453/2018-8, respectively). MASM and ES thank Brazilian Council for Scientific and Technological Development (CNPq) for research grant

#305792/2020-2 and financial support 430426/2018-6. We kindly thank Prof. J. M. Feliu for providing the single crystals employed in this work. This work used computational resources of the “Centro Nacional de Processamento de Alto Desempenho em São Paulo” (CENAPAD-SP), “Centro de Computação John David Rogers” (CCJDR-UNICAMP), and the SDumont (LNCC).

References

1 J. N. Galloway, W. H. Schlesinger, H. Levy II, A. Michaels and J. L. Schnoor, *Global Biogeochemical Cycles*, 1995, **9**, 235–252.

2 P. M. Vitousek, J. D. Aber, R. W. Howarth, G. E. Likens, P. A. Matson, D. W. Schindler, W. H. Schlesinger and D. G. Tilman, *Ecological Applications*, 1997, **7**, 737–750.

3 Y. Zeng, C. Priest, G. Wang and G. Wu, *Small Methods*, 2020, **4**, 2000672.

4 M. C. Figueiredo and I. Katsounaros, ed. K. B. T.-E. of I. C. Wandelt, Elsevier, Oxford, 2018, pp. 761–768.

5 N. Singh and B. R. Goldsmith, *ACS Catalysis*, 2020, **10**, 3365–3371.

6 N. N. Grenwood and A. B. T. Earnshaw, in *Chemistry of the Elements*, eds. N. N. Grenwood and A. B. T. Earnshaw, Elsevier, Oxford, 1997, pp. 406–472.

7 K. Nishimura, K. Machida and M. Enyo, *Electrochimica Acta*, 1991, **36**, 877–880.

8 M. C. P. M. da Cunha, J. P. I. de Souza and F. C. Nart, *Langmuir*, 2000, **16**, 771–777.

9 G. Horányi and E. M. Rizmayer, *Electrochimica Acta*, 1985, **30**, 923–926.

10 G. E. Dima, A. C. A. de Vooys and M. T. M. Koper, *Journal of Electroanalytical Chemistry*, 2003, **554–555**, 15–23.

11 O. A. Petrii and T. Ya. Safonova, *Journal of Electroanalytical Chemistry*, 1992, **331**, 897–912.

12 S. Wasmus, E. J. Vasini, M. Krausa, H. T. Mishima and W. Vielstich, *Electrochimica Acta*, 1994, **39**, 23–31.

13 A. v Rudnev, E. B. Molodkina, M. R. Ehrenburg, R. G. Fedorov, A. I. Danilov, Yu. M. Polukarov and J. M. Feliu, *Russian Journal of Electrochemistry*, 2009, **45**, 1052.

14 M. C. P. M. da Cunha, M. Weber and F. C. Nart, *Journal of Electroanalytical Chemistry*, 1996, **414**, 163–170.

15 J.-X. Liu, D. Richards, N. Singh and B. R. Goldsmith, *ACS Catalysis*, 2019, **9**, 7052–7064.

16 A. Rodes, R. Gomez, J. M. Orts, J. M. Feliu, J. M. Perez and A. Aldaz, *Langmuir*, 1995, **11**, 3549–3553.

17 I. Katsounaros, M. C. Figueiredo, X. Chen, F. Calle-Vallejo and M. T. M. Koper, *ACS Catalysis*, 2017, **7**, 4660–4667.

18 A. Clayborne, H.-J. Chun, R. B. Rankin and J. Greeley, *Angewandte Chemie International Edition*, 2015, **54**, 8255–8258.

19 G. E. Dima, G. L. Beltramo and M. T. M. Koper, *Electrochimica Acta*, 2005, **50**, 4318–4326.

20 E. B. Molodkina, I. G. Botryakova, A. I. Danilov, J. Souza-Garcia and J. M. Feliu, *Russian Journal of Electrochemistry*, 2012, **48**, 302–315.

21 I. Katsounaros, M. C. Figueiredo, X. Chen, F. Calle-Vallejo and M. T. M. Koper, *Electrochimica Acta*, 2018, **271**, 77–83.

22 M. T. de Groot and M. T. M. Koper, *Journal of Electroanalytical Chemistry*, 2004, **562**, 81–94.

23 F.-Y. Chen, Z.-Y. Wu, S. Gupta, D. J. Rivera, S. v Lambeets, S. Pecaut, J. Y. T. Kim, P. Zhu, Y. Z. Finfrock, D. M. Meira, G. King, G. Gao, W. Xu, D. A. Cullen, H. Zhou, Y. Han, D. E. Perea, C. L. Muhich and H. Wang, *Nature Nanotechnology*, , DOI:10.1038/s41565-022-01121-4.

24 G. Soffiati, J. L. Bott-Neto, V. Y. Yukuhiro, C. T. G. V. M. T. Pires, C. C. Lima, C. R. Zanata, Y. Y. Birdja, M. T. M. Koper, M. A. San-Miguel and P. S. Fernández, *The Journal of Physical Chemistry C*, 2020, **124**, 14745–14751.

25 R. B. Getman and W. F. Schneider, *The Journal of Physical Chemistry C*, 2007, **111**, 389–397.

26 J. H. Montoya, C. Tsai, A. Vojvodic and J. K. Nørskov, *ChemSusChem*, 2015, **8**, 2180–2186.

27 C. Stuhlmann, I. Villegas and M. J. Weaver, *Chemical Physics Letters*, 1994, **219**, 319–324.

28 Y.-G. Kim, S.-L. Yau and K. Itaya, *J Am Chem Soc*, 1996, **118**, 393–400.

29 F. Huerta, E. Morallón, C. Quijada, J. L. Vázquez and A. Aldaz, *Electrochimica Acta*, 1998, **44**, 943–948.

30 F. J. Huerta, E. Morallón, JoséL. Vazquez and A. Aldaz, *Surface Science*, 1998, **396**, 400–410.

31 M. Escudero-Escribano, M. E. Zoloff Michoff, E. P. M. Leiva, N. M. Marković, C. Gutiérrez and Á. Cuesta, *ChemPhysChem*, 2011, **12**, 2230–2234.

32 C. Korzeniewski, V. Climent and J. M. Feliu, *Electroanalytical Chemistry: A Series of Advances*, 2012, **24**, 75–169.

33 K. N. da Silva, R. Nagao and E. Sitta, *Electrochimica Acta*, 2020, **360**, 136986.

34 A. Cuesta, *J Am Chem Soc*, 2006, **128**, 13332–13333.

35 G. Kresse and J. Hafner, *Physical Review B*, 1993, **47**, 558–561.

36 G. Kresse and J. Furthmüller, *Computational Materials Science*, 1996, **6**, 15–50.

37 G. Kresse and J. Hafner, *Physical Review B*, 1994, **49**, 14251–14269.

38 G. Kresse and J. Furthmüller, *Physical Review B*, 1996, **54**, 11169–11186.

39 G. Kresse and D. Joubert, *Physical Review B*, 1999, **59**, 1758–1775.

40 J. P. Perdew, K. Burke and M. Ernzerhof, *Physical Review Letters*, 1996, **77**, 3865–3868.

41 P. E. Blöchl, *Physical Review B*, 1994, **50**, 17953–17979.

42 C. Kittel, *Introduction to Solid State Physics*, Wiley, 8th edn., 2004.

43 C. Wildi, G. Cabello, M. E. Zoloff Michoff, P. Vélez, E. P. M. Leiva, J. J. Calvente, R. Andreu and A. Cuesta, *The Journal of Physical Chemistry C*, 2016, **120**, 15586–15592.

44 G. Henkelman, A. Arnaldsson and H. Jónsson, *Computational Materials Science*, 2006, **36**, 354–360.

45 J. Clavilier, R. Albalat, R. Gomez, J. M. Orts, J. M. Feliu and A. Aldaz, *Journal of Electroanalytical Chemistry*, 1992, **330**, 489–497.

46 A. Cuesta and M. Escudero, *Physical Chemistry Chemical Physics*, 2008, **10**, 3628–3634.

47 S. Taguchi and J. M. Feliu, *Electrochimica Acta*, 2008, **53**, 3626–3634.

48 M. Duca, V. Kavvadia, P. Rodriguez, S. C. S. Lai, T. Hoogenboom and M. T. M. Koper, *Journal of Electroanalytical Chemistry*, 2010, **649**, 59–68.

49 A. Cuesta, *ChemPhysChem*, 2011, **12**, 2375–2385.

50 A. Rodes, R. Gómez, J. M. Pérez, J. M. Feliu and A. Aldaz, *Electrochimica Acta*, 1996, **41**, 729–745.

51 V. Rosca, G. L. Beltramo and M. T. M. Koper, *Langmuir*, 2005, **21**, 1448–1456.

52 K. Nakata, Y. Kayama, K. Shimazu, A. Yamakata, S. Ye and M. Osawa, *Langmuir*, 2008, **24**, 4358–4363.

53 F. Calle-Vallejo, M. Huang, J. B. Henry, M. T. M. Koper and A. S. Bandarenka, *Physical Chemistry Chemical Physics*, 2013, **15**, 3196–3202.

54 V. Briega-Martos, E. Herrero and J. M. Feliu, *Current Opinion in Electrochemistry*, 2019, **17**, 97–105.

55 G. A. Attard and A. Ahmadi, *Journal of Electroanalytical Chemistry*, 1995, **389**, 175–190.

56 V. Climent, G. A. Attard and J. M. Feliu, *Journal of Electroanalytical Chemistry*, 2002, **532**, 67–74.

57 J. Yang, P. Sebastian, M. Duca, T. Hoogenboom and M. T. M. Koper, *Chemical Communications*, 2014, **50**, 2148–2151.

58 M. J. S. Farias and J. M. Feliu, *Topics in Current Chemistry*, 2019, **377**, 5.

59 H. Kim, M. W. Chung and C. H. Choi, *Electrochemistry Communications*, 2018, **94**, 31–35.

60 M. T. M. Koper, S. C. S. Lai and E. Herrero, *Fuel Cell Catalysis*, 2009, 159–207.